

# On ternary species mixing and combustion in isotropic turbulence at high pressure

Hong Lou and Richard S. Miller<sup>a)</sup>

*Department of Mechanical Engineering, Clemson University, Clemson, South Carolina 29634-0921*

(Received 4 June 2003; accepted 23 January 2004; published online 5 April 2004)

Effects of Soret and Dufour cross-diffusion, whereby both concentration and thermal diffusion occur in the presence of mass fraction, temperature, and pressure gradients, are investigated in the context of both binary and ternary species mixing and combustion in isotropic turbulence at large pressure. The compressible flow formulation is based on a cubic real-gas state equation, and includes generalized forms for heat and mass diffusion derived from nonequilibrium thermodynamics and fluctuation theory. A previously derived formulation of the generalized binary species heat and mass fluxes is first extended to the case of ternary species, and appropriate treatment of the thermal and mass diffusion factors is described. Direct numerical simulations (DNS) are then conducted for both binary and ternary species mixing and combustion in stationary isotropic turbulence. Mean flow temperatures and pressures of  $\langle T \rangle = 700$  K and  $\langle P \rangle = 45$  atm are considered to ensure that all species mixtures remain in the supercritical state such that phase changes do not occur. DNS of ternary species systems undergoing both pure mixing and a simple chemical reaction of the form  $O_2 + N_2 \rightarrow 2NO$  are then conducted. It is shown that stationary scalar states previously observed for binary mixing persist for the ternary species problem as well; however, the production and magnitude of the scalar variance is found to be altered for the intermediate molecular weight species as compared to the binary species case. The intermediate molecular weight species produces a substantially smaller scalar variance than the remaining species for all flows considered. For combustion of nonstoichiometric mixtures, a binary species mixture, characterized by stationary scalar states, results at long times after the lean reactant is depleted. The form of this final scalar distribution is observed to be similar to that found in the binary flow situation. A series of lower resolution simulations for a variety of species is then used to show the dependence of the stationary scalar variance on the turbulence Reynolds number, turbulence Mach number, species molecular weight ratio, and relative proportion of two species present in the flow after completion of combustion. © 2004 American Institute of Physics. [DOI: 10.1063/1.1687411]

## I. INTRODUCTION

Turbulent fluid mixing and combustion of hydrocarbons at large pressures encountered in modern turbines, diesel engines, and rocket engines is a subject receiving relatively recent scrutiny in the literature. These devices operate at pressures larger than the thermodynamic critical pressure for a pure component (or “critical locus” for a mixture) of typical hydrocarbon fuels, for which the distinction between liquid and gaseous phases vanishes and species are referred to simply as “fluid.”<sup>1</sup> A fluid is typically considered to be “supercritical” when either its temperature or pressure is above the critical value;<sup>2</sup> however, there is some ambiguity in the literature as to whether or not both properties need to be above their critical values. From the perspective of the fluid transport physics, having either temperature or pressure fixed above critical negates the possibility of phase change. No new physics is introduced by having both values above critical conditions. Therefore for the purposes of the present in-

vestigation we use the term supercritical to designate the state of the fluid when either the temperature or pressure is fixed above critical.

Although similar to “low pressure” flows in many ways, supercritical fluid flow may be characterized by markedly differing behavior in two primary ways. First, substantial deviations from ideal gas behavior occur, requiring consideration of real gas state equations. Second, “cross-diffusion” effects by which heat diffuses in the presence of concentration and/or pressure gradients (Dufour effect) and species diffuse in the presence of temperature and/or pressure gradients (Soret effect) can also result in deviations from purely Fourier and Fickian diffusion-based formulations. The present study is a continuation of the authors’ efforts in understanding the impact of cross-diffusion on real-gas fluid mixing and combustion of hydrocarbons at elevated pressures. The reader is referred to Bellan<sup>2</sup> for a recent general review of high pressure fluid behavior. Givler and Abraham<sup>3</sup> provide an additional review of supercritical droplet vaporization and combustion.

The first numerical simulations of high pressure fluid flow to include Soret and Dufour diffusion were for single isolated and spherically symmetric droplets conducted by

<sup>a)</sup>Telephone: 864-656-6248; Fax: 864-656-4335; electronic mail: rm@clemson.edu

Curtis and Farrell.<sup>4</sup> Harstad and Bellan<sup>5-8</sup> later derived the cross-diffusion terms for binary species systems from fluctuation theory<sup>9</sup> and nonequilibrium thermodynamics.<sup>10</sup> These studies further examined the role of cross-diffusion in symmetric droplet “vaporization” at high pressures for both oxygen–hydrogen systems relevant to rocket engines, and to nitrogen–hydrocarbon mixing relevant to gas turbines and diesel engines. Their formulation was then applied to direct numerical simulations (DNS) of nonhomogeneous turbulent mixing in both two-dimensional (2D) and three-dimensional (3D) temporally developing mixing layers formed by the merging of supercritical pressure nitrogen and heptane streams.<sup>11,12</sup> Real-gas effects were accounted for with the cubic Peng–Robinson state equation due to its relative computational efficiency, and the availability of a simple correction which can be used to substantially increase its accuracy.<sup>13</sup> Results of these studies illustrate the relative effects of the thermal diffusion factors on the first and second order flow statistics, and showed qualitative agreement with experimental flow visualizations of supercritical jet mixing evolutions.<sup>14</sup>

Despite prior work in nonhomogeneous flows at supercritical pressure, several interesting Soret and Dufour diffusion induced mixing phenomena are only apparent in homogeneous turbulence for which the extent of prior research is even more limited. Miller<sup>15</sup> conducted DNS of various nitrogen–hydrocarbon mixtures in stationary isotropic compressible turbulence using the same nonequilibrium thermodynamical and real-gas formulation discussed above. They began their simulations from initially perfectly premixed binary species systems with 50/50 nitrogen with heptane, 3-methylhexane and dodecane. Unlike a typical low pressure system, the perfectly premixed species were observed to initially “anti-diffuse” due to a Soret cross diffusion induced by pressure gradients present in the compressible flow. A statistically steady scalar state was eventually achieved in each simulation through a balance between the scalar variance production due to the pressure gradient term and the traditional destructive nature of the Fickian diffusion term. The presence of the steady scalar states made the scalar variance evolution inconsistent with the traditionally observed exponential decay typical of low pressure mixing. Scalar distributions were found to be non-Gaussian and nonsymmetric due to the influence of the partial molar volume difference appearing in the pressure gradient related Soret term. The final steady state values of the scalar variance were then quantified and found to increase with increasing turbulence Mach number, molecular weight ratio of the binary species, and with decreasing turbulence Reynolds number.

Lou and Miller<sup>16</sup> then considered the impact of Soret and Dufour cross-diffusion effects on mixing and combustion through an examination of the scalar probability density function (PDF) transport equation for binary mixing in isotropic turbulence at supercritical pressure. They conducted DNS of the binary mixing case at a resolution of  $192^3$  grid points for heptane mixing with nitrogen from initially non-premixed conditions at 45 atm pressure and 700 K mean temperature. Two simulations were performed for the mixing of an initially spherical heptane “blob” in nitrogen. One case

employed the complete binary form of the Soret and Dufour cross-diffusion fluxes, whereas for the second simulation these fluxes were turned off with only “standard” forms of the Fickian and Fourier mass and heat diffusion being considered. The evolutions of the two mixing cases were found to be nearly identical for early times prior to the destruction of the pure heptane blob. However, at long times Soret diffusion due to pressure gradient proportional terms results in stationary scalar states not observed in the absence of cross-diffusion. Several new terms appearing in the PDF transport equation were identified and observed to be important to the long time scalar evolution. Several models typically used for the low pressure PDF transport equation were found to perform poorly at high pressures and relatively long times. Nevertheless, the ultimate impact of these effects on actual combustion modeling could not be determined by the purely isotropic mixing cases considered.

Based on the above discussions, the primary objectives of the present study are to: (1) extend the binary species formulation to ternary species systems, (2) conduct DNS of three species turbulent mixing in order to analyze the effects of Soret and Dufour diffusion and to compare these effects with the binary mixing problem, and (3) to conduct preliminary combustion simulations based on the new ternary species formulation as applied to a simplified chemical reaction of the form  $Fuel + Oxidizer \rightarrow Product$ . All simulations are based on an isotropic compressible “box turbulence” geometry utilizing flow forcing in order to create stationary turbulence conditions. For the purposes of this study (and for reasons discussed below), all chemical reactions are considered to be nonheat releasing. Although somewhat restrictive, both of these simplifications represent a first, and fundamental, step in the analysis of cross-diffusion effects on multi-component mixture behavior under realistic mixing and combustion conditions at high pressures. The paper is organized as follows. The formulation and numerical approach are summarized in Secs. II and III, respectively. Specification of properties is discussed in Sec. IV. Results relevant to ternary species system mixing and combustion in isotropic turbulence are the subject of Sec. V. Conclusions and further discussions are provided in Sec. VI.

## II. FORMULATION

For pressures greater than the thermodynamic critical pressure, the distinction between gaseous and liquid phases vanishes, and deviations from ideal gas behavior become significant.<sup>1,2</sup> The following formulation therefore includes conservation equations for a single phase compressible fluid mixture density, momentum, total energy (internal plus kinetic), two independent species mass fractions, as well as a real-gas state equation (described below):

$$\frac{\partial \rho}{\partial t} + \frac{\partial}{\partial x_j} [\rho u_j] = 0, \quad (1)$$

$$\frac{\partial}{\partial t} (\rho u_i) + \frac{\partial}{\partial x_j} [\rho u_i u_j + P \delta_{ij} - \tau_{ij}] = \rho F_i, \quad (2)$$

$$\frac{\partial}{\partial t}(\rho e_t) + \frac{\partial}{\partial x_j}[(\rho e_t + P)u_j - u_i \tau_{ij} + Q_j] = \rho u_i F_i, \quad (3)$$

respectively. In the above expressions,  $\rho$  is the mixture density,  $u_i$  is the velocity vector,  $P$  is the thermodynamic pressure,  $\tau_{ij}$  is the Newtonian viscous stress tensor (assumed to apply to the present fluids) with viscosity  $\mu$ ,  $e_t$  is the specific total energy,  $Q_i$  is the heat flux vector,  $\delta_{ij}$  is the Kronecker delta tensor, and  $F_i$  is an artificial “stirring” force added to maintain statistically stationary turbulence.

The conservation equations and cubic Peng–Robinson state equation for a ternary species system under supercritical considerations are nearly identical to the binary formulation given by Refs. 15 and 16. The alterations to these equations for ternary species are the form of the heat and mass flux vectors, as well as in an additional mass transport equation required to describe the system. In this case, transport equations are required for the mass fractions of two species (denoted  $Y_1$  and  $Y_2$ , respectively):

$$\frac{\partial}{\partial t}(\rho Y_1) + \frac{\partial}{\partial x_j}[\rho Y_1 u_j + J_{j,1}] = \dot{\omega}_1 \quad (4)$$

and

$$\frac{\partial}{\partial t}(\rho Y_2) + \frac{\partial}{\partial x_j}[\rho Y_2 u_j + J_{j,2}] = \dot{\omega}_2, \quad (5)$$

where  $J_{i,\alpha}$  is the mass flux vector associated with species  $\alpha$ . The third species mass fraction is given by  $Y_3 = 1 - Y_1 - Y_2$ . The above equations include the potential for a simple chemical reaction of the form *Fuel* + *Oxidizer* → *Products*. The chemical kinetics are based on the following temperature independent form of the reaction rates ( $\dot{\omega}_\alpha$ ). For the two reactants, species 1 and 2, the (irreversible) reaction rates take the forms:

$$\dot{\omega}_1 = -\rho K_R \left( \frac{M_3}{M_2} \right) Y_1 Y_2, \quad (6)$$

$$\dot{\omega}_2 = -\rho K_R \left( \frac{M_3}{M_1} \right) Y_1 Y_2, \quad (7)$$

respectively, where  $K_R$  is the constant reaction frequency and  $M_\alpha$  is the molecular weight of species  $\alpha$ . Both pure mixing ( $\dot{\omega} = 0$ ) and chemically reacting cases are considered. Note also that the ternary species derivation allows an exothermic reaction to be considered. However, for isotropic turbulence in a closed system the mean pressure will increase in the event of heat release. Therefore, only nonheat releasing reactions are considered in what follows.

### A. Thermodynamic state equation

A variety of options exist in choosing an appropriate equation of state, including complex forms such as the Benedict–Webb–Rubin and Lee–Kesler forms.<sup>1</sup> However, such state equations, though highly accurate over large regions of thermodynamic state space, are relatively complex to implement in the context of a three-dimensional computational fluid dynamics code. More computationally efficient state equations, such as cubic forms, can lead to large errors

near the critical locus; however, they usually behave well away from it. For the purposes of this study we choose the cubic Peng–Robinson state equation for the following reasons: (1) it is efficient to program, (2) only purely supercritical thermodynamic regimes away from the critical locus are considered, and (3) a simple curve fitting “fix” has been published by Harstad *et al.*<sup>13</sup> which increases its accuracy to within 1% relative error relative to Lee–Kesler (as tested for pure components). This correction could be added in a simple manner for increased accuracy if needed.

The cubic Peng–Robinson state equation is expressed as

$$P = \frac{\mathcal{R}T}{V - B_m} - \frac{A_m}{V^2 + 2VB_m - B_m^2}, \quad (8)$$

where  $\mathcal{R}$  is the universal gas constant,  $V$  is the molar volume, and  $A_m$  and  $B_m$  are mixture parameters which are defined based on appropriately chosen mixing rules. Many such sets of mixing rules have been proposed with varying degrees of accuracy under differing thermodynamic conditions.<sup>1</sup> For the purposes of this study we choose to utilize the mixing rules recommended by Harstad *et al.*:<sup>13</sup>

$$A_m = \sum_\alpha \sum_\beta X_\alpha X_\beta A_{\alpha\beta}, \quad (9)$$

$$B_m = \sum_\alpha X_\alpha B_\alpha, \quad (10)$$

$$A_{\alpha\beta} = 0.457236(\mathcal{R}T_{\alpha\beta}^c)^2 \times [1 + C_{\alpha\beta}(1 - \sqrt{T/T_{\alpha\beta}^c})]^2 / P_{\alpha\beta}^c, \quad (11)$$

$$B_\alpha = 0.077796\mathcal{R}T_{\alpha\alpha}^c / P_{\alpha\alpha}^c, \quad (12)$$

$$C_{\alpha\beta} = 0.37464 + 1.54226\Omega_{\alpha\beta} - 0.26992\Omega_{\alpha\beta}^2, \quad (13)$$

based on their accuracy for hydrocarbons and their consistency with the above described available correction to the state equation. In the above, the superscript  $c$  refers to critical properties (i.e.,  $T/T^c$  is the “reduced” temperature). The diagonal elements of the “critical matrices” are equal to their pure substance counterparts; i.e.,  $T_{\alpha\alpha}^c = T_\alpha^c$ ,  $P_{\alpha\alpha}^c = P_\alpha^c$ , and  $\Omega_{\alpha\alpha} = \Omega_\alpha$  where  $\Omega$  is the acentric factor of species  $\alpha$ . The off-diagonal elements are evaluated using additional mixing rules:

$$T_{\alpha\beta}^c = \sqrt{T_{\alpha\alpha}^c T_{\beta\beta}^c} (1 - k_{\alpha\beta}), \quad (14)$$

$$P_{\alpha\beta}^c = Z_{\alpha\beta}^c (\mathcal{R}T_{\alpha\beta}^c / V_{\alpha\beta}^c),$$

$$V_{\alpha\beta}^c = \frac{1}{8} [(V_{\alpha\alpha}^c)^{1/3} + (V_{\beta\beta}^c)^{1/3}]^3, \quad (15)$$

$$Z_{\alpha\beta}^c = \frac{1}{2} (Z_{\alpha\alpha}^c + Z_{\beta\beta}^c), \quad \Omega_{\alpha\beta} = \frac{1}{2} (\Omega_{\alpha\alpha} + \Omega_{\beta\beta}),$$

where the diagonal elements of each of the above symmetric matrices are also equal to the pure substance values. The binary interaction parameter,  $k_{\alpha\beta}$ , is a function of the species being considered and is taken to be  $k_{\alpha\beta} = 0.1$  for  $\alpha \neq \beta$  and  $k_{\alpha\alpha} = 0$  for the binary mixtures addressed in this study.

In order to ensure self-consistency, all of the thermodynamic parameters of the flow should be calculated from the same equation of state. For the present fluid dynamics simulations the variables of interest are the molar enthalpy ( $H$ ), the constant pressure molar heat capacity ( $C_p$ ), the partial molar enthalpy ( $H_{,\alpha}$ ), the partial molar volume ( $V_{,\alpha}$ ), and the speed of sound ( $a_s$ ). Each of these functions can be obtained through various derivatives and functions of the Gibbs energy.<sup>1,17</sup> Derived forms for these parameters have been previously published in Refs. 11, 15, and 16 for arbitrary numbers of species.

**B. Ternary species heat and mass flux vectors**

The derivation of the heat and mass flux vectors for multicomponent mixtures is based on Keizer’s fluctuation-dissipation theory which is developed from a fundamental theory of fluid drop behavior under supercritical conditions by Harstad and Bellan.<sup>5,8</sup> The model of Harstad and Bellan describes nonequilibrium processes and constructs a substantially more general relationship for thermodynamic heat and mass fluxes than equilibrium theory provides. The fluctuation-dissipation theory additionally shows that the modeling of transport processes is consistent with nonequilibrium thermodynamics. The resulting form of the mass flux is a superposition of Fickian and Soret diffusion, whereas the heat flux is a superposition of Fourier and Dufour diffusion. A detailed derivation of the following heat and mass flux vectors is available in Ref. 18.

As in our previous investigations,<sup>15,16</sup> the final forms for the heat and mass fluxes are expressed as a superposition of separate flux vectors proportional to gradients of mass (or mole) fractions, temperature, and pressure. The heat flux vectors and the mass-based mass flux vectors are further decomposed into terms proportional to each of the individual species 1 and 2 mole fraction gradients (denoted by superscripts  $Y_1$  and  $Y_2$ ):

$$Q_j = Q_j^T + Q_j^{Y_1} + Q_j^{Y_2} + Q_j^P, \tag{16}$$

and

$$J_{j,\alpha} = J_{j,\alpha}^{Y_1} + J_{j,\alpha}^{Y_2} + J_{j,\alpha}^T + J_{j,\alpha}^P, \tag{17}$$

where  $\alpha$  denotes the particular species.

The resulting final forms for the heat flux components referred to throughout the remainder of this work are

$$Q_j^T = - \left\{ \kappa + \mathcal{R} \frac{M_m^2}{M_1 M_2} Y_1 Y_2 n D_m^{(12)} \alpha_{IK}^{(12)} \alpha_{BK}^{(12)} + \mathcal{R} \frac{M_m^2}{M_1 M_3} Y_1 Y_3 n D_m^{(13)} \alpha_{IK}^{(13)} \alpha_{BK}^{(13)} + \mathcal{R} \frac{M_m^2}{M_2 M_3} Y_2 Y_3 n D_m^{(23)} \alpha_{IK}^{(23)} \alpha_{BK}^{(23)} \right\} \nabla T, \tag{18}$$

$$Q_j^{Y_1} = -n \mathcal{R} T \{ Y_2 \alpha_{IK}^{(12)} D_m^{(12)} \alpha_D^{(11)} + Y_1 \alpha_{IK}^{(21)} D_m^{(21)} \alpha_D^{(21)} + Y_3 \alpha_{IK}^{(13)} D_m^{(13)} \alpha_D^{(11)} + Y_1 \alpha_{IK}^{(31)} D_m^{(31)} \alpha_D^{(31)} + Y_3 \alpha_{IK}^{(23)} D_m^{(23)} \alpha_D^{(21)} + Y_2 \alpha_{IK}^{(32)} D_m^{(32)} \alpha_D^{(31)} \} \nabla X_1, \tag{19}$$

$$Q_j^{Y_2} = -n \mathcal{R} T \{ Y_2 \alpha_{IK}^{(12)} D_m^{(12)} \alpha_D^{(12)} + Y_1 \alpha_{IK}^{(21)} D_m^{(21)} \alpha_D^{(22)} + Y_3 \alpha_{IK}^{(13)} D_m^{(13)} \alpha_D^{(12)} + Y_1 \alpha_{IK}^{(31)} D_m^{(31)} \alpha_D^{(32)} + Y_3 \alpha_{IK}^{(23)} D_m^{(23)} \alpha_D^{(22)} + Y_2 \alpha_{IK}^{(32)} D_m^{(32)} \alpha_D^{(32)} \} \nabla X_2, \tag{20}$$

and

$$Q_j^P = -n M_m \left\{ Y_1 Y_2 \alpha_{IK}^{(12)} D_m^{(12)} \left( \frac{V_{,1}}{M_1} - \frac{V_{,2}}{M_2} \right) + Y_1 Y_3 \alpha_{IK}^{(13)} D_m^{(13)} \left( \frac{V_{,1}}{M_1} - \frac{V_{,3}}{M_3} \right) + Y_2 Y_3 \alpha_{IK}^{(23)} D_m^{(23)} \left( \frac{V_{,2}}{M_2} - \frac{V_{,3}}{M_3} \right) \right\} \nabla P, \tag{21}$$

respectively. In the above,  $X_\alpha$  is the mole fraction of species  $\alpha$  (related to the mass fraction through  $M_\alpha X_\alpha = M_m Y_\alpha$ , where  $M_m = \sum X_\alpha M_\alpha$  is the mixture molecular weight),  $n = V^{-1}$  is the molar density,  $\kappa$  is the form of the thermal conductivity consistent with kinetic theory,  $D_m^{(ij)} = D_m^{(ji)}$  are the binary mass diffusivities between species  $i$  and  $j$ , and  $V_{,i} = \partial V / \partial X_i$  is the partial molar volume (the partial molar enthalpy is  $H_{,i} = \partial H / \partial X_i$ ). In addition,  $\alpha_{IK}^{(ij)} = -\alpha_{IK}^{(ji)}$  and  $\alpha_{BK}^{(ij)} = -\alpha_{BK}^{(ji)}$  are the similarly defined ‘‘Irving–Kirkwood’’ and ‘‘Bearman–Kirkwood’’ forms of the thermal diffusion factors, respectively, and  $\alpha_D^{(ij)}$  are the mass diffusion factors (see below).

The corresponding mass flux vector components for species 1 are

$$J_{j,1}^{Y_1} = -n \frac{M_1}{M_m} \{ M_2 Y_2 D_m^{(12)} \alpha_D^{(11)} + M_3 Y_3 D_m^{(13)} \alpha_D^{(11)} - M_2 Y_1 D_m^{(12)} \alpha_D^{(21)} - M_3 Y_1 D_m^{(13)} \alpha_D^{(31)} \} \nabla X_1, \tag{22}$$

$$J_{j,1}^{Y_2} = -n \frac{M_1}{M_m} \{ M_2 Y_2 D_m^{(12)} \alpha_D^{(12)} + M_3 Y_3 D_m^{(13)} \alpha_D^{(12)} - M_2 Y_1 D_m^{(12)} \alpha_D^{(22)} - M_3 Y_1 D_m^{(13)} \alpha_D^{(32)} \} \nabla X_2, \tag{23}$$

$$J_{j,1}^T = -M_m \frac{n}{T} \{ Y_1 Y_2 D_m^{(12)} \alpha_{BK}^{(12)} + Y_1 Y_3 D_m^{(13)} \alpha_{BK}^{(13)} \} \nabla T, \tag{24}$$

and

$$J_{j,1}^P = -\frac{n M_1}{\mathcal{R} T} \left\{ M_2 Y_1 Y_2 D_m^{(12)} \left( \frac{V_{,1}}{M_1} - \frac{V_{,2}}{M_2} \right) + M_3 Y_1 Y_3 D_m^{(13)} \left( \frac{V_{,1}}{M_1} - \frac{V_{,3}}{M_3} \right) \right\} \nabla P, \tag{25}$$

respectively, whereas those for species 2 are

$$J_{j,2}^{Y_1} = -n \frac{M_2}{M_m} \left\{ -M_1 Y_2 D_m^{(12)} \alpha_D^{(11)} + M_1 Y_1 D_m^{(12)} \alpha_D^{(21)} + M_3 Y_3 D_m^{(23)} \alpha_D^{(21)} - M_3 Y_2 D_m^{(23)} \alpha_D^{(31)} \right\} \nabla X_1, \quad (26)$$

$$J_{j,2}^{Y_2} = -n \frac{M_2}{M_m} \left\{ -M_1 Y_2 D_m^{(12)} \alpha_D^{(12)} + M_1 Y_1 D_m^{(12)} \alpha_D^{(22)} + M_3 Y_3 D_m^{(23)} \alpha_D^{(22)} - M_3 Y_2 D_m^{(23)} \alpha_D^{(32)} \right\} \nabla X_2, \quad (27)$$

$$J_{j,2}^T = -M_m \frac{n}{T} \left\{ Y_2 Y_3 D_m^{(23)} \alpha_{BK}^{(23)} - Y_1 Y_2 D_m^{(12)} \alpha_{BK}^{(12)} \right\} \nabla T, \quad (28)$$

and

$$J_{j,2}^P = -\frac{nM_2}{RT} \left\{ M_1 Y_1 Y_2 D_m^{(12)} \left( \frac{V_{,2}}{M_2} - \frac{V_{,1}}{M_1} \right) + M_3 Y_2 Y_3 D_m^{(23)} \left( \frac{V_{,2}}{M_2} - \frac{V_{,3}}{M_3} \right) \right\} \nabla P, \quad (29)$$

respectively. The above forms apply to the remainder of this work, and are the forms applied to the computational fluid dynamics code described below. If required, the mass flux vector  $J_{j,3}$  can be calculated in mass form based on the conservation principle:

$$\sum_{\alpha} J_{i,\alpha} = 0. \quad (30)$$

The above derivation has been checked to reduce to the binary species flux formulations presented in Refs. 15 and 16.

### C. Heat and mass diffusion factors

Three additional thermodynamic relations appear in the above expressions. The parameters  $\alpha_{JK}$  and  $\alpha_{BK}$  are referred to as the ‘‘Irving–Kirkwood’’ and the ‘‘Bearman–Kirkwood’’ forms of the thermal diffusion factor,<sup>11,19</sup> respectively. These two factors are related to one another through an expression derived by Harstad and Bellan:<sup>8</sup>

$$\alpha_{JK}^{(ij)} = \alpha_{BK}^{(ij)} + \frac{1}{RT} \frac{M_i M_j}{M_m} \left( \frac{H_{,i}}{M_i} - \frac{H_{,j}}{M_j} \right). \quad (31)$$

Equation (31) implies that only one of these parameters needs to be specified based on the specific species under consideration; the other is then known implicitly through the above equation.

The mass diffusion factors  $\alpha_D^{(ij)}$  are related to molar gradients of the fugacity; their form can be derived given a specific equation of state:

$$\alpha_D^{(ij)} = \frac{\partial X_i}{\partial X_j} + X_i \frac{\partial \ln \gamma_i}{\partial X_j}, \quad (32)$$

where  $\gamma_i$  is the activity coefficient of the mixture. The Gibbs–Duhem relation,

$$\sum_{i=1}^N \sum_{j=1}^{N-1} \alpha_D^{(ij)} dX_j = 0, \quad (33)$$

where  $N$  is the total number of species, puts a further restriction on the diffusion factors. For a binary species system, the

above relations result in only a single independent mass diffusion factor denoted  $\alpha_D$  having a relatively complex form as derived from the Peng–Robinson state equation. For the purposes of the present study the derivation of the corresponding form of the mass diffusion factors from the Peng–Robinson state equations is exceedingly complex. As an alternative, we model the mass diffusion factors based on the assumption of ideal mixing behavior in which case the activity coefficient is independent of the concentration.<sup>17</sup> In this case, an examination of Eqs. (32) and (33) yields

$$\alpha_D^{(11)} = \alpha_D^{(22)} = 1, \quad (34)$$

$$\alpha_D^{(31)} = \alpha_D^{(32)} = -1, \quad (35)$$

$$\alpha_D^{(12)} = \alpha_D^{(21)} = 0. \quad (36)$$

Miller<sup>15</sup> observed that for binary mixtures under conditions relevant to the present investigation the (single) mass diffusion factor is near unity ( $\alpha_D$  varied from 0.82 to 0.94 for different cases examined in that study). In order to test the validity of the ideal mixing assumption, several binary mixing cases from Ref. 15 were repeated using  $\alpha_D = 1$ . The results in all cases were nearly identical to the previously published trends therefore providing justification for the present approach to ternary species systems.

### III. NUMERICAL APPROACH

The above equations are solved for the case of isotropic box turbulence in a triply periodic domain having equal lengths  $L$  in each of the three coordinate directions;  $x_1$ ,  $x_2$ , and  $x_3$ . Statistically stationary turbulent flow is maintained via the addition of an artificial forcing term added to the momentum and energy equations having a form originally proposed by Kida and Orszag.<sup>20</sup> The governing equations are solved using a third order Runge–Kutta time advancement procedure coupled with eighth order accurate central finite differencing for all spatial derivatives.<sup>21</sup> Tenth order accurate explicit filtering is applied to the primitive variables at each Runge–Kutta stage to control numerical oscillations in the solution. An eighth order accurate central finite difference scheme<sup>21</sup> was chosen due to its high accuracy, zero numerical diffusion, ease of parallelization, and previously published results for similar single and two-phase simulation.<sup>15,16,22–24</sup> During each simulation, the ratio of  $\eta/\Delta x$  is monitored to remain greater than unity as a resolution check. All thermodynamic conditions met during the simulations are carefully monitored to ensure that the critical locus is not approached in order to avoid phase changes which would violate the single phase fluid formulation. Energy spectra are also examined to ensure monotonic decrease of energy at high wave numbers. Mass balances are also checked thoroughly as further evidence that the complex mass flux vectors are evaluated correctly. Finally, the code was checked by reproducing ‘‘low pressure’’ simulation results of Kida and Orszag.<sup>20</sup> The specifics of the forcing routine, as well as additional details relating to the numerical methodology as well as to code validation can be found in Refs. 15 and 18.

### Evaluation of the state equation

A cubic real-gas state equation must in general be solved iteratively to get both the temperature and pressure simultaneously (given the density, internal energy, and mass fractions). However, in order to avoid costly iterations Miller<sup>15</sup> derived a highly accurate curve fit for the specific internal energy of the mixture ( $e_i$ ) over the entire state space of interest. This approach has been extended by the authors for the ternary species problem, thus requiring a four-dimensional curve fitting [ $e_i = e_i(\rho, T, Y_1, Y_2)$ ]

$$\left( \frac{e_i - e_L}{e_U - e_L} \right) = C_1 \left( \frac{T - T_L}{T_U - T_L} \right) + C_2 \left( \frac{T - T_L}{T_U - T_L} \right)^2, \quad (37)$$

which can be solved explicitly for the temperature via the quadratic formula. In the above expression

$$\left( \frac{e_L - e^{(1)}}{e^{(2)} - e^{(1)}} \right) = C_3 \left( \frac{\rho - \rho_L}{\rho_U - \rho_L} \right) + C_4 \left( \frac{\rho - \rho_L}{\rho_U - \rho_L} \right)^2, \quad (38)$$

$$\left( \frac{e_U - e^{(3)}}{e^{(4)} - e^{(3)}} \right) = C_5 \left( \frac{\rho - \rho_L}{\rho_U - \rho_L} \right) + C_6 \left( \frac{\rho - \rho_L}{\rho_U - \rho_L} \right)^2, \quad (39)$$

where the subscripts  $L$  and  $U$  correspond to the lower and upper limits of the parameter space, respectively. And the four internal energy functions  $e^{(1)}(Y_1, Y_2; T_L, \rho_L)$ ,  $e^{(2)}(Y_1, Y_2; T_L, \rho_U)$ ,  $e^{(3)}(Y_1, Y_2; T_U, \rho_L)$ , and  $e^{(4)}(Y_1, Y_2; T_U, \rho_U)$  are

$$\left( \frac{e^{(\alpha)} - e_L^{(\alpha)}}{e_U^{(\alpha)} - e_L^{(\alpha)}} \right) = C_7^{(\alpha)} Y_2 + C_8^{(\alpha)} Y_2^2; \quad \alpha = 1, 2, 3, 4. \quad (40)$$

Finally, the eight remaining internal energy functions  $e_L^{(\alpha)}$  and  $e_U^{(\alpha)}$  can be expressed:

$$\left( \frac{e_L^{(\alpha)} - e'^{(\alpha)}}{e''^{(\alpha)} - e'^{(\alpha)}} \right) = C_9^{(\alpha)} Y_1 + C_{10}^{(\alpha)} Y_1^2; \quad \alpha = 1, 2, 3, 4. \quad (41)$$

$$\left( \frac{e_U^{(\alpha)} - e'''^{(\alpha)}}{e''^{(\alpha)} - e'''^{(\alpha)}} \right) = C_{11}^{(\alpha)} Y_1 + C_{12}^{(\alpha)} Y_1^2; \quad \alpha = 1, 2, 3, 4. \quad (42)$$

In practice each of the parameters  $C_1 \rightarrow C_{12}$  is obtained by a least mean square error (LMSE) solution. In determining all of the parameters, the “error” is measured relative to the Peng–Robinson predicted value. In this case, a perfect curve fit will reproduce the Peng–Robinson state equation behavior exactly, yet will not require any numerical iterations to implement in a computational fluid dynamics code. Note also that nothing in the fitting procedure limits its use to the Peng–Robinson state equation. The procedure can be used with any state equation with equal simplicity (including the “corrected” Peng–Robinson equation mentioned above).

The procedure for applying the curve fit is as follows. First, a range of temperature, mass fraction, and pressure (and therefore density) is input which encompasses the thermodynamic state space under consideration. Then the 16 constants  $C_9^{(\alpha)} \rightarrow C_{12}^{(\alpha)}$  are determined using the LMSE analysis where the error is evaluated relative to the Peng–Robinson predicted value. This allows the other eight constants  $C_7^{(\alpha)}$  and  $C_8^{(\alpha)}$  to be calculated. Then the  $e_L$  and  $e_U$

coefficients ( $C_3, C_4, C_5, C_6$ ) can be solved. Finally, another separate application of the LMSE procedure determines the remaining coefficients  $C_1$  and  $C_2$ . The final curve fit, Eq. (37), can then be written in forms which are explicit in either the temperature or the internal energy. The fit can therefore be used to determine both the internal energy during initialization (for consistency), as well as to calculate the temperature from the internal energy during each time step.

The entire curve fitting process is performed during the initialization of the code automatically and requires negligible computational effort. Furthermore, the state space range can be checked dynamically during each simulation. If this range ever extends beyond the input range the curve fit is simply recalculated. Application of the procedure was found to produce highly accurate fits for the temperature as a function of the internal energy for all of the cases considered in this study. For example, for typical ternary species problems the thermodynamic state space chosen for the fit was  $0 \leq Y_1 \leq 1$ ,  $0 \leq Y_2 \leq 1$ ,  $500 \text{ K} \leq T \leq 1250 \text{ K}$ , and  $25 \text{ atm} \leq p \leq 100 \text{ atm}$ . Two sets of error estimates are defined to test the accuracy of the curve fitting procedure. The “relative error” is defined as the average root-mean-square (rms) difference between the predicted temperature extracted from the curve fit for some input set of internal energy, density, and mass fractions, with the actual Peng–Robinson predicted temperature, and divided by the actual Peng–Robinson temperature. The “maximum error” is defined as the corresponding maximum absolute temperature difference throughout the entire thermodynamic state space used for the curve fit. As example mixtures, the following three case were studied: (1) nitrogen, heptane, and dodecane, (2) heptane, 3-methylhexane, and 2-methylhexane, and (3) nitrogen, oxygen, and nitric oxide. The resulting relative errors for these mixtures are 0.34%, 0.23%, and 0.22%, respectively. The corresponding maximum errors are approximately 25.0, 8.2, and 8.4 K, respectively. However, an examination of where in thermodynamic state space these maximum errors appear reveals that they occur at the extremes of temperature and pressure; conditions which are rarely, if ever, attained during actual simulations. It was therefore concluded that the curve fitting procedure provides a sufficiently accurate representation of the Peng–Robinson state equation behavior under all conditions relevant to this study. It should also be noted that the term “error” is somewhat misleading in the present context. Any error present does not, in the strict sense, contaminate the solution. Such an error would only produce a deviation in the effective form of the state equation without any internal inconsistency in the code.

### IV. PROPERTIES

The molecular weights, critical temperatures and pressures, and acentric factors for all species considered in this study are provided in Table I. The particular species appearing in the table were chosen based on their relevance to typical mixing and combustion problems. Various combinations of these species will be used below to study the influence of molecular weight ratios on the mixing process, as well as to mimic a typical “simple” three species chemical

TABLE I. Molecular weight, critical temperature and pressure, and acentric factor for all species considered in the study.

Species	$M$	$T^C$ (K)	$p^C$ (atm)	$\Omega$
Nitrogen	28.013	126.26	33.46	0.039
Heptane	100.205	540.3	27.04	0.349
Dodecane	170.34	658.2	17.96	0.575
3-methylhexane	100.205	535.3	27.73	0.323
2-methylhexane	100.205	530.4	26.94	0.329
Oxygen	31.999	154.6	49.74	0.025
Nitric oxide	30.006	180.0	63.95	0.588

reaction. Diffusive properties are modeled in a simplified manner and are assumed to be species independent in order to simplify the analyses. For example, using the true mixture viscosity, which is a function of temperature, pressure, and mixture composition (as are thermal conductivities and mass diffusivities), is not possible for realistic length scales due to inherent resolution restrictions on three-dimensional DNS. Furthermore, only relatively restricted information exists on the behavior of these properties for the large pressures considered in the present study.<sup>1</sup> Therefore, in order to simplify the analysis, the mixture viscosity ( $\mu$ ) is assumed to be constant and is calculated based on a specified value of the “box Reynolds number,”  $Re_0 = \rho_0 U_0 L_0 / \mu$ , based on reference values for the density, velocity, and length. This treatment of viscosity also allows for an easier delineation of effects specifically due to Soret and Dufour diffusion without the superposition of second order effects due to viscosity variations. Similarly, the thermal conductivity and mass diffusivity are calculated from specified constant values of the Prandtl [ $Pr = \mu / (\rho C_p \kappa)$ ] and Schmidt [ $Sc = \mu / (\rho D)$ ] numbers;  $Pr = Sc = 0.7$ . Again, with limited knowledge of the behavior of mass and thermal diffusivities at elevated pressures and temperatures, we opt for a simplified fundamental study of Soret and Dufour effects under well defined viscous and diffusive conditions. A forthcoming investigation will focus on realistic detailed treatments of these fluid properties for one-dimensional laminar and exothermic flames for which completely resolved simulations are possible.

Chemical reactions are specified by the following non-dimensional parameters. The Damkohler number  $Da$  is defined as the ratio of the characteristic time scale of the flow to the characteristic reaction time scale:  $Da(T) = K_R L_0 / U_0$ . For the purposes of the present study, only nonheat releasing and constant rate chemical reactions are considered. For the present simulations, the reference density is set equal to the mean density in the domain ( $\rho_o = \langle \rho \rangle$ ), the reference velocity scale is taken equal to the acoustic velocity ( $a$ ) based on the initial mean thermodynamic parameters ( $U_0 = a_0$ ), the reference length scale is  $L_0 = L / (2\pi)$ , and the reference temperature is equal to the initial mean flow temperature ( $T_0 = \langle T \rangle_0$ ).

Finally, either of the Irving–Kirkwood or the Bearman–Kirkwood forms of the thermal diffusion coefficients must be specified to close the formulation. The exact nature of these parameters remains poorly understood; therefore a somewhat simplified approach is taken to defining these parameters

(see Miller *et al.*<sup>11</sup> for a parametric study of the effect of varying the thermal diffusion factors in a binary species mixing layer configuration). For binary species pairs, a molecular weight ratio based correlation<sup>4</sup> was used to specify the Irving–Kirkwood form of the thermal diffusion factor in Refs. 15 and 16. This correlation yields values consistent with the choice of thermal diffusion factor shown to yield good comparisons with experimental data for supercritical heptane spherical droplet vaporization in nitrogen in Ref. 8. Therefore the above correlation can be extended to ternary species diffusion factors with relative confidence:

$$\alpha_{IK}^{(ij)} = 2.3842 \times 10^{-2} + 0.248 \, 21 \log_{10} \left[ \max \left( \frac{M_i}{M_j}, \frac{M_j}{M_i} \right) \right], \quad (43)$$

i.e., applied to the species pairs to which each component of  $\alpha_{IK}^{(ij)}$  is applied.

## V. RESULTS

The primary focus of the present investigation is ternary species mixing and chemical reaction in compressible isotropic turbulence under supercritical conditions. As discussed above, the long time scalar variance is an increasing function of the molecular weight ratio for binary mixtures. In this paper, we extend the investigation to ternary mixtures in order to determine if such stationary scalar states continue to exist, and if so, in what form for the various species present. Furthermore, the ability to treat three species enables the consideration of a simple chemical reaction of the form *Fuel* + *Oxidizer* → *Product* which will enable us to begin to understand the potential role of Soret and Dufour diffusion in high pressure turbulent flames.

For each simulation presented in what follows, an initial turbulent flow is first prepared by integrating the governing equations until a stationary flow state is achieved. For these preparation simulations the scalars are initialized as perfectly premixed with relative masses corresponding to those of the final simulation for which the initialization is intended. The base mean temperature and pressure is identical for all cases;  $T = 700$  K and pressure  $P = 45$  atm ( $a_0$  is based on these conditions), respectively. The simulations parameters for the first portion of this study are provided in Table II.

Unless otherwise specified, all simulations are conducted using  $128^3$  numerical grid points, and have mean Mach number, Taylor microscale based Reynolds number, and relative resolution of  $M_C \approx 0.2$ ,  $Re_\lambda \approx 52$ , and  $\eta/\Delta x \approx 1.44$ , respectively (note that this is a “quasi-stationary” state for compressible flow due to viscous dissipation effects increasing the mean internal energy with time<sup>15,20</sup>). The ensemble averaged (over all grid points) Mach number is defined as  $M_C = \langle (u_i u_i)^{1/2} / a \rangle$ . The Reynolds number is defined as  $Re_\lambda = \langle \rho \rangle \langle u_i u_i \rangle [5 / (3 \mu \epsilon_u)]^{1/2}$ , where the velocity dissipation is  $\epsilon_u = \mu \langle \omega_i \omega_i \rangle + 4/3 \mu \langle (\partial u_i / \partial x_i)^2 \rangle$  ( $\omega_i$  is the vorticity vector). The resulting stationary velocity flow field is characterized by a mean Kolmogorov length scale ( $\eta$ ) which is larger than the grid spacing; where  $\eta = [(\mu^3 / (\epsilon_u \langle \rho \rangle^2))]^{1/4}$ .

Once the stationary state is achieved, the scalar fields for the mixing cases (denoted by  $Da = 0$ ; i.e., runs 1, 2, and 3 in

TABLE II. Simulation parameters and initial conditions (S/D indicates inclusion of the Soret and Dufour diffusion terms). All simulations are conducted using  $128^3$  grid points, and have mean  $M_C \approx 0.20$ ,  $Re_\lambda \approx 52$ , and  $\eta/\Delta x \approx 1.44$ .

Run	Species 1	Species 2	Species 3	S/D	$Da$	$\langle Y_1 \rangle$	$\langle Y_2 \rangle$
1	Nitrogen	Heptane	Dodecane	Yes	0	1/3	1/3
2	Heptane	3-methylhexane	2-methylhexane	Yes	0	1/3	1/3
3	Oxygen	Nitrogen	Nitric oxide	Yes	0	1/3	1/3
4	Oxygen	Nitrogen	Nitric oxide	Yes	1	0.5	0.5
5	Oxygen	Nitrogen	Nitric oxide	No	1	0.5	0.5
6	Oxygen	Nitrogen	Nitric oxide	Yes	1	0.75	0.25

Table II) are reinitialized as perfectly premixed mixtures having  $Y_1 = Y_2 = Y_3 = 1/3$  everywhere in the domain. In the case of chemically reacting flows (runs 4, 5, and 6) we choose to examine a simple reaction of the form  $N_2 + O_2 \rightarrow 2NO$  due to its relevant occurrence in hydrocarbon combustion, as well as to the fact that it involves only three species and can therefore be modeled using the previously described heat and mass flux formulation. The simulation procedure is identical to the binary “droplet” cases studied by Lou and Miller.<sup>16</sup> That is, the scalar field is reinitialized to produce a single spherical “droplet” of pure nitrogen fluid embedded in a pure oxygen environment. Within the “droplet,” the mean temperature is again reduced by 50 K to create initial temperature gradients, and an error function profile is used to smooth the transition gradients (including temperature and mass fraction) between the nitrogen and oxygen. The premixed  $O_2$  and  $N_2$  at the “droplet” interface is converted to a thin layer of product species (NO). This is done so that there are no premixed reactants in the initial conditions which could result in artificially large local reaction rates with the potential for resolution problems. All cases involving chemical reactions have a Damkohler number  $Da = 1$ .

### A. Ternary mixing

The simulations described in Table II are first used to investigate the influence of Soret and Dufour effects on supercritical fluid mixing. In particular, runs 1–3 are used to illustrate the influence of the molecular weight distribution of the ternary species from completely premixed nonreacting initial conditions. Run 1 is a nitrogen, heptane, dodecane mixture with molecular weights equal to 28.013, 100.205, and 170.34, respectively, and has the largest variation in molecular weights (see Table I). Run 2 is a heptane, 3-methylhexane, 2-methylhexane mixture with equal molecular weights ( $M = 100.205$ ). Run 3 is another pure mixing simulation conducted due to its relevance to the reacting cases described next. It is an oxygen, nitrogen, nitric oxide mixture having molecular weights 31.999, 28.013, and 30.006, respectively. Note that the critical pressures of oxygen and nitric oxide are both larger than the ambient flow pressure; however, both species are in their supercritical states as presently defined due to the larger than critical flow temperature (see Table I).

### 1. Ternary mixing and scalar variance evolution

In contrast to typical “low pressure” behavior, the presence of both temperature and pressure gradients in the compressible flow results in nonzero mass flux vectors at initial times, despite the initial species fields being perfectly premixed [see Eqs. (23)–(29)]. For the purposes of this study, the relative intensity of the scalar fluctuations is expressed in terms of the Favre averaged standard deviation,  $\langle\langle Y'' Y'' \rangle\rangle^{1/2}$  (averaging is over the spatial ensemble). Figure 1 presents the temporal evolutions of the standard deviations of all species for mixing cases runs 1–3. Time is nondimensionalized as  $t^* = tU_0/L_0$ . In all cases, the standard deviations of the species mass fractions begin to grow from zero at early times, and then evolve steadily towards stationary values as observed previously for the binary mixing problem. However, in contrast to the binary species problem in which case both species mass fractions are characterized by identical standard deviations, the stationary values displayed in Fig. 1 are not all equal. For the two cases composed of nonequal molecular weight species [Figs. 1(a) and 1(c)] the largest and smallest molecular weight species have nearly identical scalar variance. However, the intermediate molecular weight species has a stationary scalar standard deviation approximately one order of magnitude smaller than the other two species. In contrast, for the case of nearly equal molecular weight species [Fig. 1(b)] an approximately equal final state of the scalar distribution is reached for all three species.

Molecular weight is not the only parameter affecting the equation of state and the heat and mass flux formulations. The relative magnitude of the final scalar variance for heptane, 3-methylhexane, and 2-methylhexane in Fig. 1(b) is inversely proportional to the critical pressures of the three species (see Table I). Further testing would need to be performed before this relationship could be confirmed to yield the observed behavior (however, it may be difficult to find ternary species which all have the same molecular weight with large differences in critical pressures). One additional observation from Fig. 1 is that the scalar standard deviation indeed increases with increasing diversity in the molecular weights of the chosen species; in agreement with the results for binary species mixing.

In order to further illustrate the nature of the scalar fluctuation evolution, Fig. 2 depicts the temporal evolution of the instantaneous minima and maxima of each species mass fraction for run 1. Although the standard deviations are relatively

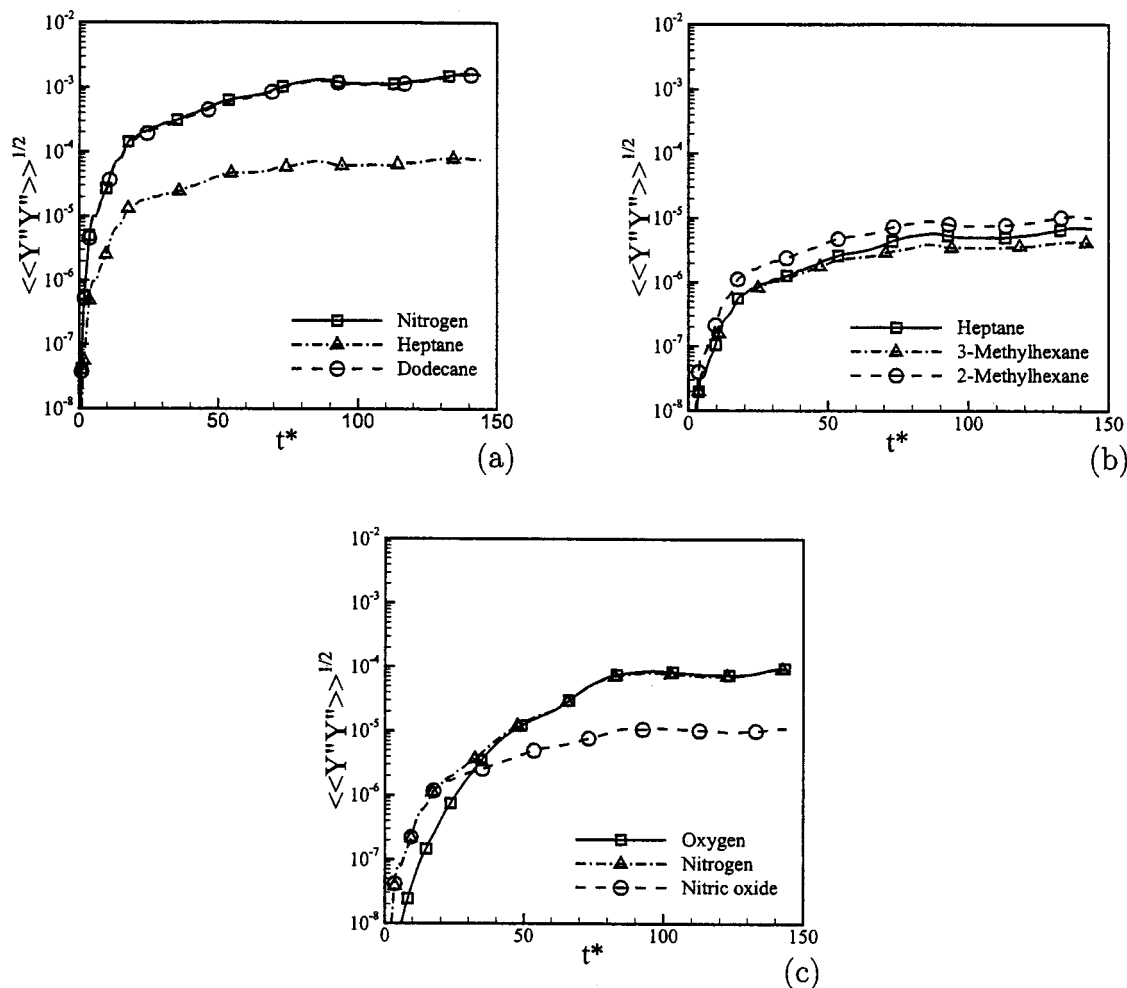


FIG. 1. Temporal evolution of the Favre averaged standard deviation for each mass fraction for (a) run 1, (b) run 2, and (c) run 3.

small compared to the scalar mean ( $\langle Y_1 \rangle = \langle Y_2 \rangle = \langle Y_3 \rangle = 1/3$ ), the magnitude of the fluctuations is relatively significant as observed by the long time minima and maxima in the figure. Again, the largest and smallest molecular weight species exhibit the widest variations in the mass fraction extrema, with nearly negligible variation for the intermediate molecular weight species; heptane. In addition, a clear skew-

ness is observed for the nitrogen and dodecane; towards large mass fractions for the low molecular weight nitrogen, and towards small mass fractions for the large molecular weight dodecane. As with the binary mixing problem, this skewness can be attributed to a skewness in the partial molar volume difference appearing in the definitions of  $J_{j,\alpha}^P$ .

The skewness in the scalar distributions is further illustrated through the long time PDF of the scalar mixture fraction ( $\phi$ ) defined in this case based on the species 1 and 2 mass fractions;  $0 \leq \phi = (Y_1 - Y_2 + 1)/2 \leq 1$ . The mixture fraction is “conserved” in the sense that its transport equation does not contain any reaction source terms even for the case of combustion. In this manner, the evolution of  $\phi$  is identical for isothermal reacting flows for any value of the Damkohler number (including the pure mixing case,  $Da=0$ ). For this reason the mixture fraction is an important parameter in the study of reacting flows, and many turbulent combustion models aim to predict its evolution.

Figure 3 presents the long time ( $t^*=150$ ) PDF of the mixture fraction distribution for cases runs 1–3. As shown earlier for binary mixture scalars, the PDF of the mixture fraction demonstrates a clear and inherent skewness in the scalar mass fraction distributions. Also in agreement with previous binary species results are the near exponential tails

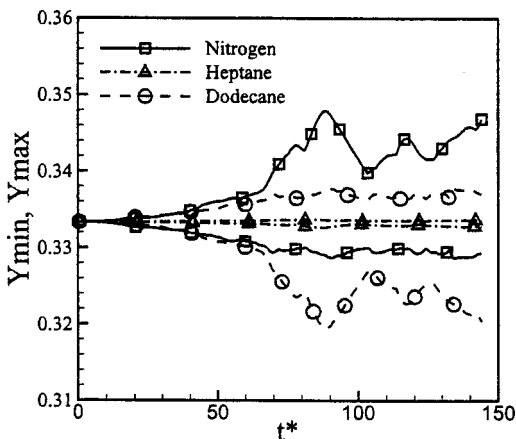


FIG. 2. Temporal evolution of the minimum and maximum mass fractions for run 1.

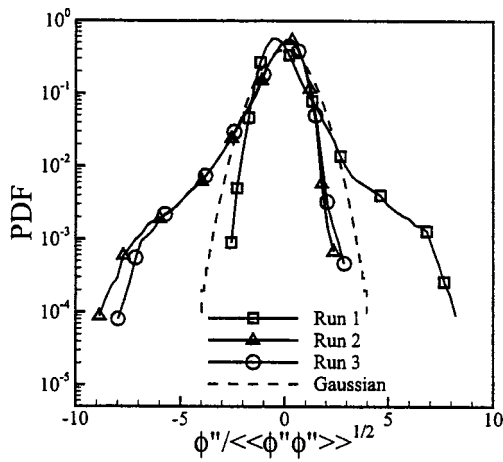


FIG. 3. Probability density function of the normalized mixture fraction Favre fluctuation at time  $t^* = 150$  for runs 1–3.

exhibited by each of the distributions on its skewed side. Note also that the sign of the skewness portrayed by each of the PDFs is arbitrary, and is determined exclusively by the choice of species 1 and 2 in the definition of the mixture fraction based on their relative molecular weights. A reversal in the species denoted 1 and 2 will simply reflect the distribution about its mean (normalized to zero in the figure). The potential impact of these asymmetries in the scalar distributions on PDF based turbulent combustion models was addressed in Ref. 16 for the case of the binary mixing problem. Since these models are often applied to the evolution of the conserved mixture fraction, which can be defined similarly for either binary or ternary mixing and reaction, the conclusions of Ref. 16 in this regard will extend to the present ternary species problem. Therefore a similar analysis of conditional expectations will not be repeated in the present section.

**2. Scalar variance budget evolution**

The mechanisms responsible for the generation and maintenance of long time stationary scalar distributions for

the ternary species mixing problem are investigated through an examination of the budget evolutions for the (Favre averaged) scalar variances:

$$\frac{d}{dt} \left[ \langle \rho \rangle \frac{\langle\langle Y_1'' Y_1'' \rangle\rangle}{2} \right] = \left\langle J_{j,1}^{Y_1} \frac{\partial Y_1}{\partial x_j} \right\rangle + \left\langle J_{j,1}^{Y_2} \frac{\partial Y_1}{\partial x_j} \right\rangle + \left\langle J_{j,1}^T \frac{\partial Y_1}{\partial x_j} \right\rangle + \left\langle J_{j,1}^P \frac{\partial Y_1}{\partial x_j} \right\rangle, \quad (44)$$

$$\frac{d}{dt} \left[ \langle \rho \rangle \frac{\langle\langle Y_2'' Y_2'' \rangle\rangle}{2} \right] = \left\langle J_{j,2}^{Y_1} \frac{\partial Y_2}{\partial x_j} \right\rangle + \left\langle J_{j,2}^{Y_2} \frac{\partial Y_2}{\partial x_j} \right\rangle + \left\langle J_{j,2}^T \frac{\partial Y_2}{\partial x_j} \right\rangle + \left\langle J_{j,2}^P \frac{\partial Y_2}{\partial x_j} \right\rangle, \quad (45)$$

for species 1 and 2, respectively. The budget evolutions for each of these equations is presented in Fig. 4 as a function of nondimensional time for simulation run 1. For this simulation, species 1 is nitrogen with the lowest molecular weight, and species 2 is heptane with the intermediate molecular weight. Note that the maximum budget values are smaller for the heptane in Fig. 4(b) than for the nitrogen in Fig. 4(a). This is consistent with the smaller long time scalar variances reported for heptane in Fig. 1 due to its intermediate molecular weight compared to nitrogen and dodecane as discussed earlier.

The evolution of the various terms in the variance budget for the nitrogen species [Fig. 4(a)] follows the previously observed trends for binary species. That is, the pressure gradient induced mass flux term acts as a dominant production term in the variance transport equation budget, and is balanced at long times by the Fickian term  $J_{j,1}^{Y_1}$  due to nitrogen mass fraction gradients (note that the pressure gradients associated with this flow are induced by compressibility effects, and not by an imposed mean gradient). Both the temperature gradient induced flux and the heptane mass fraction gradient induced flux have negligible affect on the scalar variance budget. In contrast, the variance budget for the mass fraction of the heptane, with its intermediate molecular weight for this simulation, shows a very different behavior

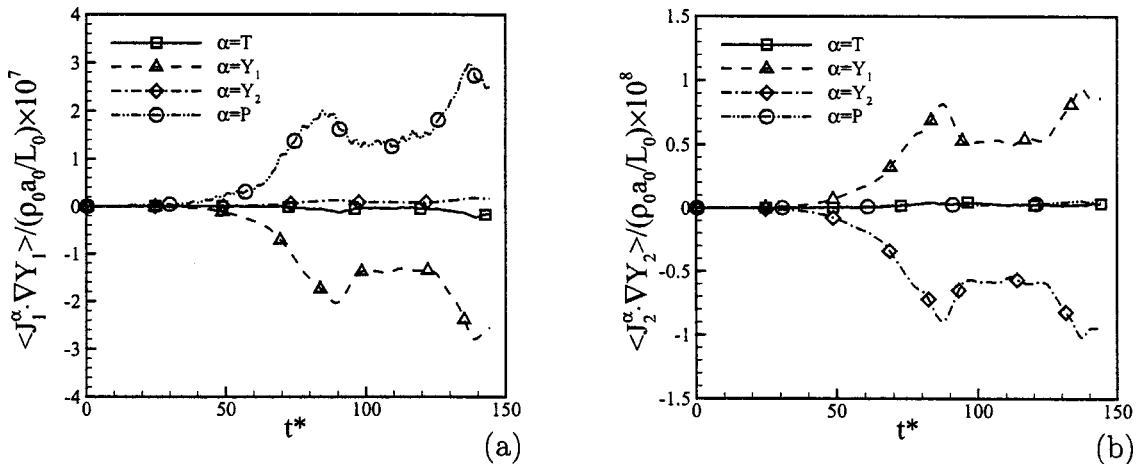


FIG. 4. Favre averaged scalar variance budget evolution for run 1 for (a) nitrogen and (b) heptane.

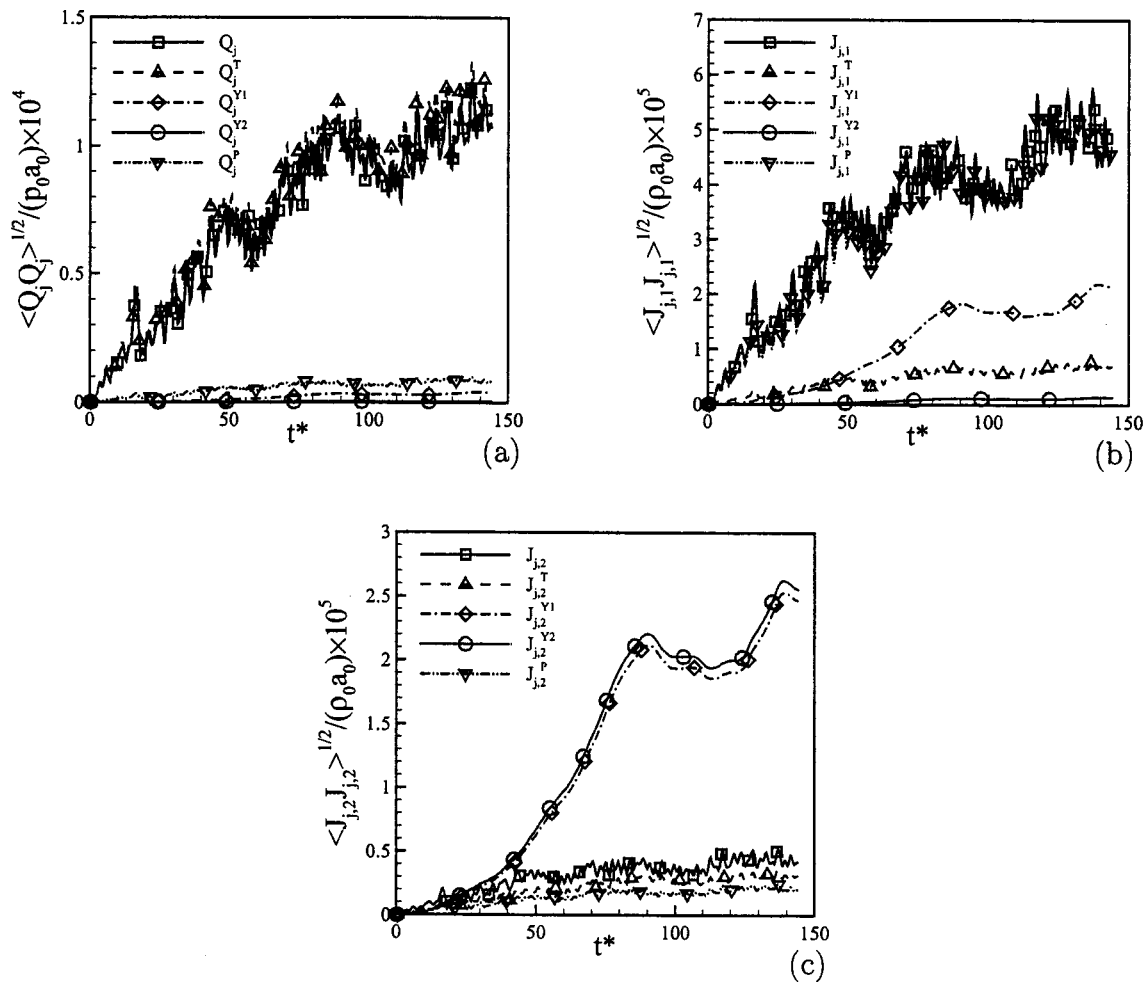


FIG. 5. Temporal evolution of heat and mass flux vector magnitudes for run 1.

not previously observed for binary mixtures. In this case, both the temperature and the pressure gradient dependent fluxes result in negligible contribution to the stationary long time heptane distribution. Rather, the long time state is observed to result from a statistical balance between production effects emanating from the nitrogen mass fraction dependent flux term (cross-species effects due to  $J_{j,1}^{Y1}$ ) and dissipation from the Fickian  $J_{j,2}^{Y2}$  flux due to heptane mass fraction gradients. Although not measured during the simulations, it is expected that the budget for the high molecular weight dodecane species would mirror the trends observed for nitrogen.

A comparison of the forms of the nitrogen and heptane pressure induced mass flux vectors [Eqs. (25) and (29), respectively] shows that the partial molar volume difference is minimized for the case of an intermediate molecular weight species (heptane) since its molecular weight is relatively near to the values of both other species. On the other hand, the relatively large molecular weight difference between nitrogen and dodecane would result in a relatively large partial molar volume difference appearing in  $J_{j,1}^P$ .

### 3. Heat and mass flux magnitude evolution

The relative effects of the Dufour and Soret cross-diffusion on the heat and mass flux vectors are examined in

Fig. 5, which depicts the magnitudes of all five vectors in each of Eqs. (16) and (17). The temporal evolution of these vector magnitudes is presented in the figure for simulation run 1, and can be used to gain further insight into the trends of Fig. 4 discussed above. The heat flux vector magnitudes in Fig. 5(a) indicate that only the temperature gradient dependent term has significant impact on the total heat flux magnitude for this particular flow. Note, however, that this trend may be altered for flows with sustained large species gradients, such as a mixing layer formed between two species; additional research in this area is warranted before general conclusions may be drawn.

The mass flux vector magnitude evolutions for the nitrogen [Fig. 5(b)] and heptane [Fig. 5(c)] support the observations made above concerning the scalar variance evolution. In particular, the pressure and nitrogen gradient dependent fluxes are the two largest subvectors for the nitrogen mass flux. The temperature gradient flux also has significant magnitude at long times; however, as shown previously,<sup>15</sup> is generally poorly correlated with gradients of the nitrogen mass fraction, therefore minimizing its impact on the scalar variance budget. On the other hand, the relative impacts of the mass flux subvectors for the heptane species reveals differing trends. In this case, the only two relatively large magnitude

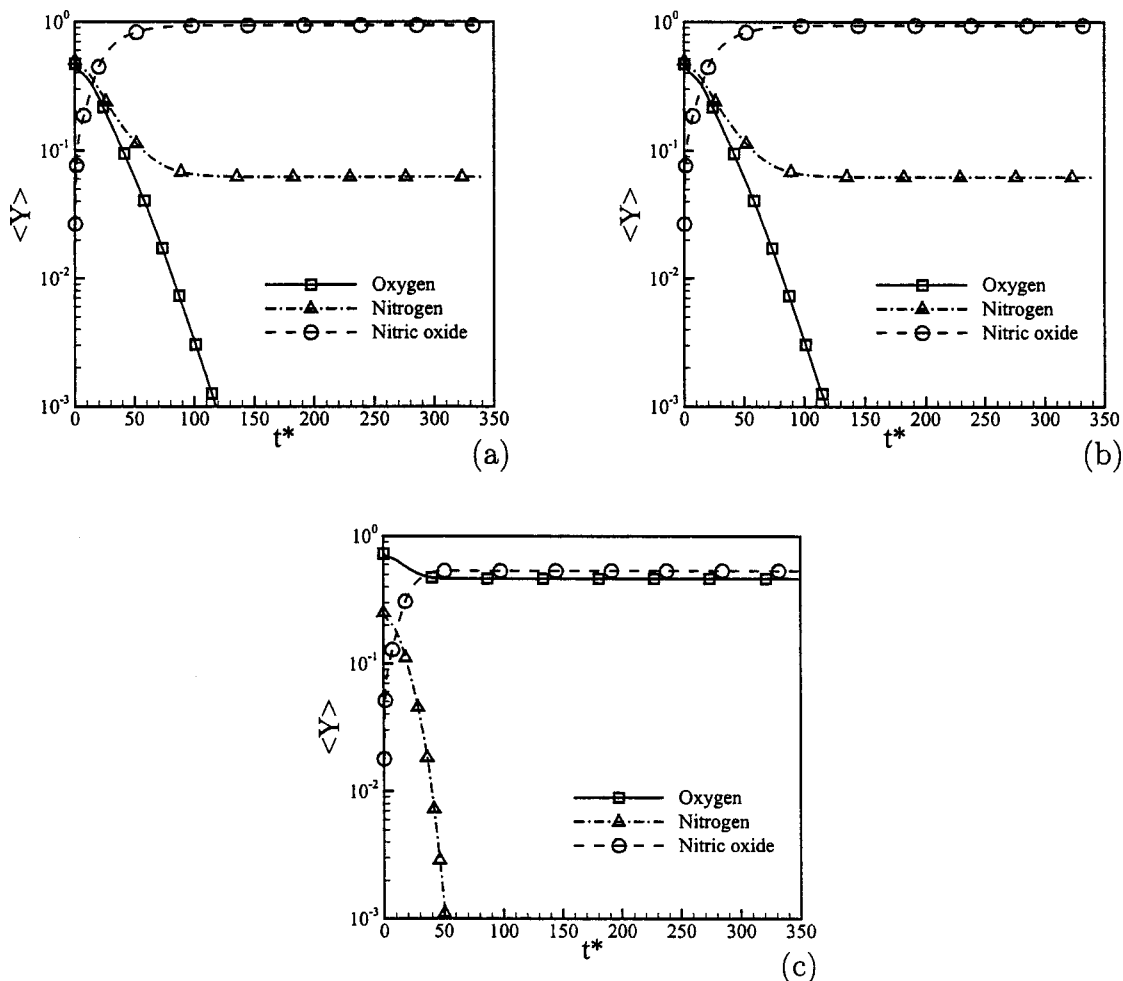


FIG. 6. Temporal evolution of mean mass fraction for (a) run 4, (b) run 5, and (c) run 6.

vectors revealed in Fig. 5(c) are those due to  $J_{j,2}^{Y_1}$  and  $J_{j,2}^{Y_2}$ ; i.e., those due to nitrogen and heptane concentration gradients, respectively. Note, however, that the total vector magnitude is in this case much smaller (square symbols), reflecting an anticorrelation in  $J_{j,2}^{Y_1}$  and  $J_{j,2}^{Y_2}$ . Such an anticorrelation reducing the overall mass flux of heptane would also promote smaller scalar variance for the heptane species as observed previously (Fig. 1).

## B. Nonpremixed chemically reacting flow

Attention is now turned towards simple nonexothermic chemically reacting flows from nonpremixed initial scalar distributions. Oxygen, nitrogen, and nitric oxide are again used for runs 4–6 (Table II) which involve the chemical reaction of an initially spherical “blob” of nitrogen reacting with an oxygen environment to form nitric oxide. The nitrogen fuel “blob” is initially centered in the domain otherwise filled with pure oxygen oxidizer; with no product nitric oxide initially present. Runs 4 and 5 both begin with 50/50 mass mixtures of fuel and oxidizer, and are identical except that Soret and Dufour diffusion are turned off for run 5 for the sake of comparison. Note that the species distribution is nonstoichiometric due to the molecular weights of  $O_2$  and  $N_2$  being nonequal. Therefore some of the lighter (nitrogen) re-

actant will remain even after complete combustion. Run 6 investigates the influence of a substantially fuel lean flow having a 75/25 mass mixture of oxygen with nitrogen. These cases represent an initial step in the investigation of high pressure turbulent flames. Consideration of additional reacting species, exothermic chemistry, and nonhomogeneous flames is delayed for future study.

### 1. Scalar reaction and moment evolution

The temporal evolution of the mean and standard deviation for each of the three scalar mass fractions for simulation runs 4–6 is presented in Figs. 6 and 7, respectively. As mentioned above, runs 4 and 5 are slightly fuel rich due to the relatively smaller molecular weight of nitrogen in comparison with oxygen. Therefore combustion in each of these simulations does not yield a single species product (nitric oxide) distribution at long times. Instead, a binary mixture results for long times characterized by nearly pure NO with a relatively small amount of  $N_2$  remaining present [Figs. 6(a) and 6(b)]. No obvious difference is observed in the mean scalar evolutions for runs 4 and 5, which are only distinguished by the absence of the Soret and Dufour cross-diffusion effects in run 5. Therefore, under the present conditions, it does not appear that Soret and Dufour diffusion

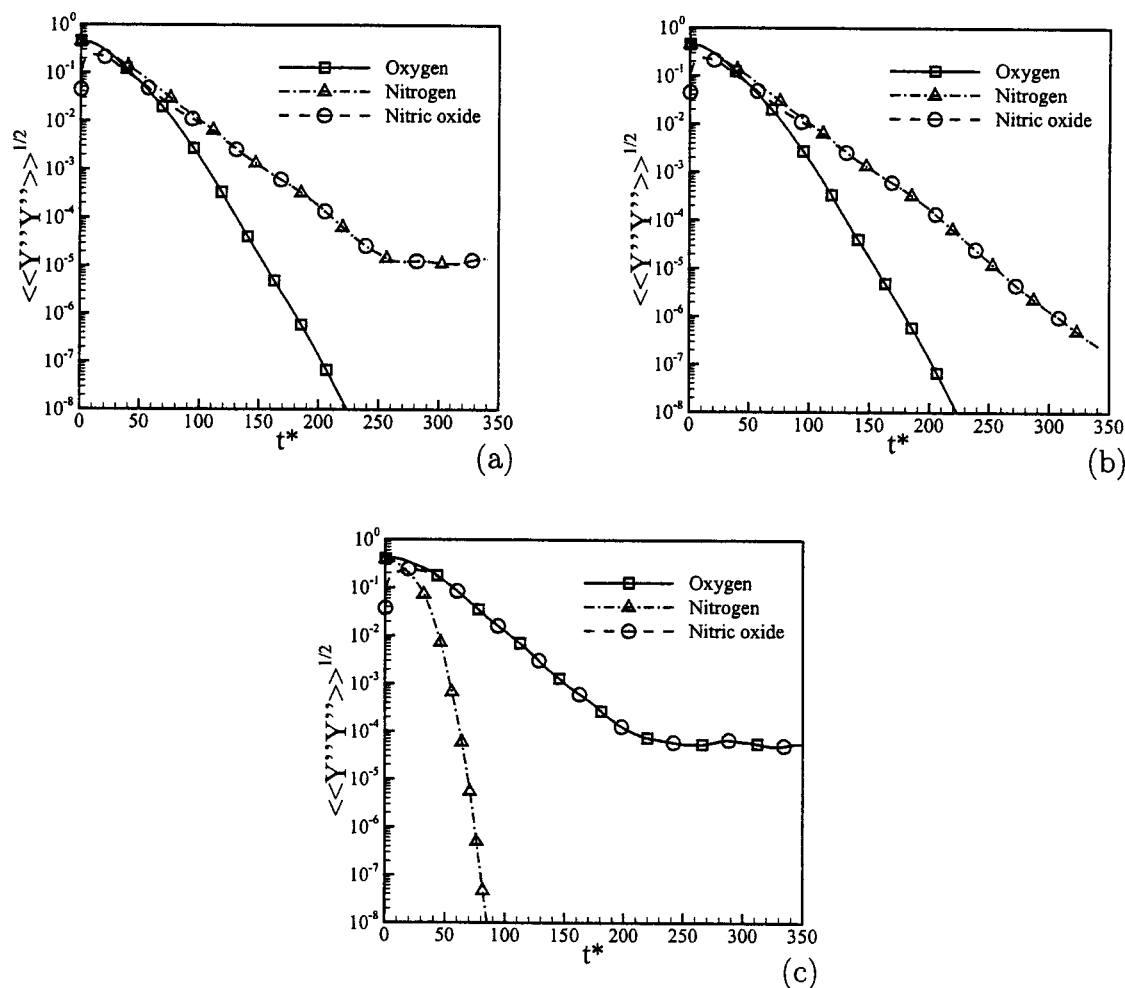


FIG. 7. Temporal evolution of Favre averaged mass fraction standard deviations for (a) run 4, (b) run 5, and (c) run 6.

have significant impact on the first order scalar moment evolutions. However, Soret and Dufour effects will be shown below to be minimized for mixture compositions near the pure species limits for a binary mixture (Fig. 9). In fact, the results for binary mixtures are highly relevant to the long time development of the present reacting flow problem, since a binary species mixture is asymptotically achieved. The results of run 6 depicted in Fig. 6(c) further illustrate this point. For this flow, the initial scalar field is markedly fuel lean. In this case, the long time scalar distribution is that of a nearly 50/50 by mass mixture of  $O_2$  and product species NO.

The development of the scalar standard deviations for runs 4–6 evolves in a similar manner (Fig. 7). An examination of the standard deviation evolutions for runs 4 and 5 in Figs. 7(a) and 7(b) illustrates the potential impact of Soret and Dufour diffusion for chemically reacting flows. Run 5 exhibits the typically observed “low pressure” behavior, in that the scalar variance decays near exponentially and indefinitely as the eventual binary species mix. In contrast, in the presence of Soret and Dufour diffusion, the scalar variance of the two remaining species ( $N_2$  and NO) decay only until the production mechanism described previously begins to reach a balance with Fickian dissipation. At this point, the scalar variance becomes stationary indicating the indefinite presence of scalar fluctuations. A similar situation occurs for

run 6 [Fig. 7(c)] with substantially larger scalar variance due to the near equal masses of species comprising the new binary mixture. With these observations, an analysis of binary mixtures could then be used to predict the ultimate scalar variance for various reactions by knowing the degree of non-stoichiometry of the initial species distribution; and therefore predicting the composition of the ultimate binary mixture. In fact, all of the above-described results for binary mixtures will apply to this ultimate scalar state for reacting flows of the form under consideration.

## 2. Scalar probability density function evolution

As a final point in the illustration of reacting flow evolution, the PDFs of the scalar mixture fraction are presented in Fig. 8 for each of simulation runs 4–6 at nondimensional times  $t^*=5$ ,  $t^*=40$ ,  $t^*=100$ , and  $t^*=300$ . The PDFs evolve from initially “double delta” distributions indicating the initially nonpremixed reactants through nearly Gaussian states at intermediate times, in agreement with “low pressure” behavior. However, at longer times [Fig. 8(c)] an obvious skewness is observed for the distributions, with near exponential tails. This is again in agreement with previous observations for the binary mixing problem.

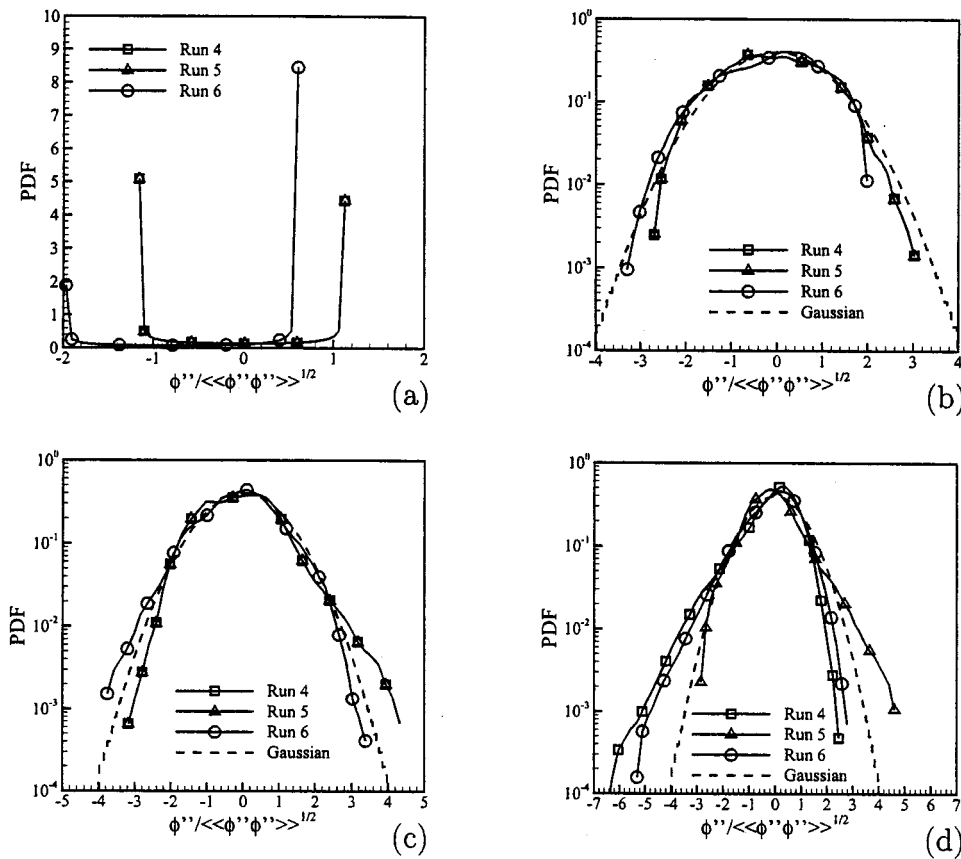


FIG. 8. Probability density function of the normalized mass fraction Favre fluctuations for runs 4–6 at times (a)  $t^* = 5$ , (b)  $t^* = 40$ , (c)  $t^* = 100$ , and (d)  $t^* = 300$ .

### 3. Mean long time scalar variance dependence

As mentioned previously, Miller<sup>15</sup> first identified the existence of long time stationary scalar variance in supercritical binary mixtures in isotropic compressible turbulence. Their simulations only addressed cases for which the binary species were initially perfectly premixed, and only 50/50 by mass mixtures were considered. They observed that the long time stationary scalar variance increased with both increasing Mach number and molecular weight ratio; however, decreased with increasing turbulence Reynolds number. As discussed above, the same phenomena of long time stationary scalar variance is observed for the present initially nonpremixed reacting flows. Our results further show that this long time state is independent of whether premixed or nonpremixed initial conditions are chosen.

In order to further quantify the long time scalar variance states, a series of simulations is conducted at a relatively lower resolution of  $64^3$  grid points for various values of the mean Reynolds number, turbulence Mach number, binary species combinations, and nitrogen mass composition (including pure single species nitrogen or hydrocarbon flows). These calculations are performed with the present ternary species code run for binary species pairs. As mentioned above, the present code was fully validated for the limiting cases of binary species pairs through comparisons with the previously published results of Ref. 15. The long time Favre averaged values of the nitrogen scalar standard deviation are presented in Fig. 9 as a function of the mean nitrogen fraction for varying Taylor microscale Reynolds number [Fig. 9(a)], turbulence Mach number [Fig. 9(b)], and binary spe-

cies pairs (i.e., molecular weight ratio) [Fig. 9(c)]. Each data point in Fig. 9 corresponds to the long time averaged value obtained for an individual simulation. Unless otherwise noted, all simulations have mean values of  $Re_\lambda \approx 35$ ,  $M_C \approx 0.2$ , and are nitrogen/heptane mixtures. In addition, the parameters for all simulations were chosen such that the condition  $\eta/\Delta x \geq 1$  is maintained in order to ensure adequate numerical resolution.

The trends observed in Fig. 9 confirm the qualitative findings of Miller<sup>15</sup> for the dependence of the scalar variance on the turbulence Reynolds number, Mach number, and molecular weight ratio. Although the DNS is by nature limited to only relatively low Reynolds numbers, the results of Fig. 9(a) still show that increasing the relative viscosity increases the level of scalar fluctuations. In addition, these results illustrate the dependence of the long time scalar variance on the mean composition of the mixture. In particular, and as expected, the limiting behavior of either pure nitrogen ( $Y_A = 1$ ) or pure hydrocarbon ( $Y_A = 0$ ) results in zero scalar variance; i.e., pure species turbulent fluids do not spontaneously produce the presence of a second fluid. It is also noted that the maximum value for the scalar variance does not occur for 50/50 mixtures by mass. In fact, the curves are in all cases skewed towards the lower molecular weight species; in this case nitrogen (when plotted as a function of mole fraction the results are also skewed towards  $X_A = 1$ ). As discussed by Miller,<sup>15</sup> the primary source of scalar variance generation for binary mixtures comes from the pressure gradient dependent mass flux vector,  $J_i^P$ . Miller<sup>15</sup> attributed observed skewness in the scalar PDF to an inherent skewness in

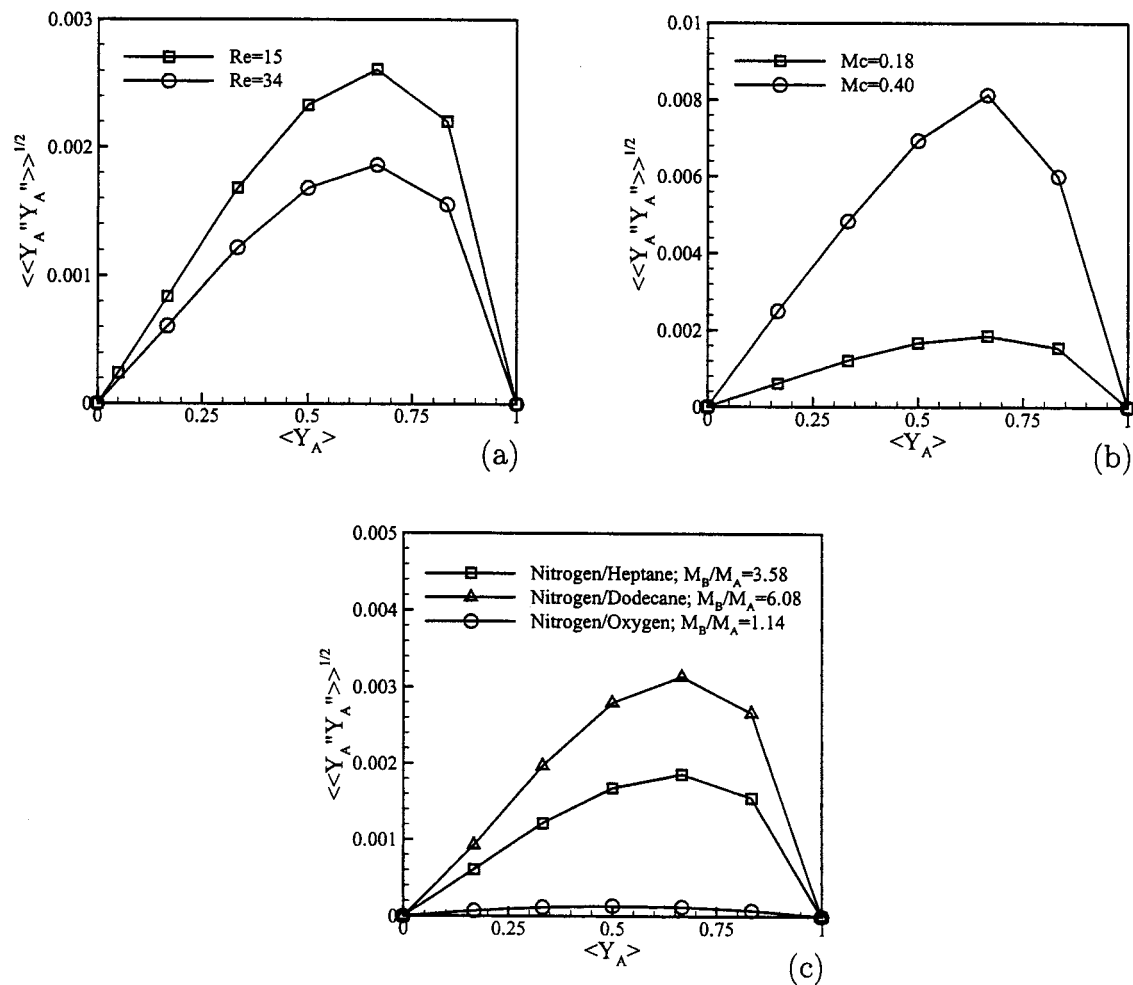


FIG. 9. Mean long time Favre averaged scalar standard deviation as a function of the mean nitrogen fraction for varying (a) Taylor microscale Reynolds number, (b) Mach number, and (c) molecular weight ratio. Unless otherwise noted, all simulations have mean values of  $Re_\lambda \approx 35$ ,  $Mc \approx 0.2$ , and are nitrogen/heptane mixtures.

the partial molar volume difference appearing in the definition of  $J_i^P$ . For the present investigation we have confirmed that this same skewness in the partial molar volume term is responsible for the observed skewness as a function of mean concentration depicted in Fig. 9.

## VI. CONCLUSIONS

High resolution direct numerical simulations (DNS) have been conducted for both binary and ternary species mixing and combustion in isotropic compressible turbulence at large pressure. The simulations are based on generalized forms of the heat and mass flux vector including Soret and Dufour cross-diffusion as derived from nonequilibrium thermodynamics and fluctuation theory. Derivation of the ternary species forms of the flux vectors has been performed by the authors, and has not appeared previously in the literature to our knowledge. Additional real-gas effects are included in the formulation via the cubic Peng–Robinson state equation based on an appropriate set of mixing rules. All thermodynamic parameters of interest have been derived directly from the state equation for self-consistency of the formulation (with the exception of the mass diffusion factors which were

derived from an assumed ideal mixing behavior). In addition, a four-dimensional curve fitting procedure has been developed by the authors in order to provide for an accurate and efficient (noniterative) application of the real-gas state equation in the DNS. Results of the simulations were presented for both ternary species mixing and combustion with a simple nonexothermic reaction of the form  $Fuel + Oxidizer \rightarrow Products$ , as well as for various binary species mixtures aimed at quantifying the long time behavior of reacting systems.

Simulations involving ternary species mixing and reaction were conducted in order to begin to understand the potential influence of Soret and Dufour diffusion on high pressure turbulent combustion. Long time statistically stationary scalar distributions, similar to those observed previously for the binary mixing problem, were observed for three initially perfectly premixed species mixing simulations. As for the binary species problem, the long time scalar variance was found to increase with increasing diversity of the molecular weights of the species. However, in contrast to the binary problem, a minimum stationary scalar variance was found for the species with intermediate molecular weight. The na-

ture of this minimum value was then elucidated based on an examination of the Favre averaged scalar variance transport equation budget and the temporal evolution of the various mass flux vector magnitudes.

For the case of reacting flow, a simple nonexothermic reaction of the form  $O_2 + N_2 \rightarrow 2NO$  was considered from nonpremixed initial conditions. The destruction of two species due to the reaction was observed to yield an eventual binary species state. Therefore at long times chemically reacting flows again yield stationary scalar states at finite times; however, the time required to reach this state is longer than in the binary species results. This final state is also characterized by stationary scalar variance and by asymmetric scalar PDFs exhibiting exponential tails. It is observed that Soret and Dufour effects are minimal for the early destruction of reactants under the nonheat releasing reaction conditions investigated.

Despite the obvious effects of Soret and Dufour diffusion on the results presented above, the ultimate impact on low order moment turbulent combustion models is probably minimal at the "early" times of interest during which the bulk of reactant conversion occurs. This does not, however, detract from the scientific interest in understanding the behavior of fluid mixing and combustion at high pressures. Future research in this area should be aimed at investigating other flow and combustion problems which may be characterized by even stronger Soret and Dufour effects. For example, an individual local flame displays sustained and relatively large temperature and concentration gradients. Nonhomogeneous flows, such as a turbulent reacting mixing layer formed between cold fuel and hot oxidizer, will also show sustained strong temperature and species gradients potentially amplifying cross diffusion effects to the point of significantly affecting turbulent combustion models. Further efforts in this area are therefore clearly warranted.

## ACKNOWLEDGMENTS

This research was supported by the National Science Foundation through the Faculty Early Career Development Program; Grant No. CTS-9983762. Computational support was provided by the California Institute of Technology's Center for Advanced Computing Research (CACR) utilizing the Hewlett-Packard V2500 and by a beowulf cluster operated by the Department of Mechanical Engineering at Clemson University.

<sup>1</sup>R. C. Reid, J. M. Prausnitz, and B. E. Poling, *The Properties of Gases and Liquids* (McGraw-Hill, Boston, MA, 1989).

- <sup>2</sup>J. Bellan, "Supercritical (and subcritical) fluid behavior and modeling: Drops, streams, shear and mixing layers, jets and sprays," *Prog. Energy Combust. Sci.* **26**, 329 (2000).
- <sup>3</sup>S. D. Givler and J. Abraham, "Supercritical droplet vaporization and combustion studies," *Prog. Energy Combust. Sci.* **22**, 1 (1996).
- <sup>4</sup>E. W. Curtis and P. V. Farrell, "A numerical study of high-pressure droplet vaporization," *Combust. Flame* **90**, 85 (1992).
- <sup>5</sup>K. G. Harstad and J. Bellan, "Isolated fluid oxygen drop behavior in fluid hydrogen at rocket chamber pressures," *Int. J. Heat Mass Transfer* **41**, 3537 (1998).
- <sup>6</sup>K. G. Harstad and J. Bellan, "Interactions of fluid oxygen drops in fluid hydrogen at rocket chamber pressures," *Int. J. Heat Mass Transfer* **41**, 3551 (1998).
- <sup>7</sup>K. G. Harstad and J. Bellan, "The Lewis number under supercritical conditions," *Int. J. Heat Mass Transfer* **42**, 961 (1999).
- <sup>8</sup>K. G. Harstad and J. Bellan, "An all pressure fluid-drop model applied to a binary mixture: Heptane in nitrogen," *Int. J. Multiphase Flow* **26**, 1675 (2000).
- <sup>9</sup>J. Keizer, *Statistical Thermodynamics of Nonequilibrium Processes* (Springer-Verlag, New York, 1987).
- <sup>10</sup>S. R. De Groot and P. Mazur, *Non-Equilibrium Thermodynamics* (Dover, New York, 1984).
- <sup>11</sup>R. S. Miller, K. G. Harstad, and J. Bellan, "Direct numerical simulation of supercritical fluid mixing layers applied to heptane-nitrogen," *J. Fluid Mech.* **436**, 1 (2001).
- <sup>12</sup>N. A. Okong'o and J. Bellan, "Direct numerical simulation of a transitional supercritical binary mixing layer: Heptane and nitrogen," *J. Fluid Mech.* **464**, 1 (2002).
- <sup>13</sup>K. G. Harstad, R. S. Miller, and J. Bellan, "Efficient high pressure state equations," *AIChE J.* **43**, 1605 (1997).
- <sup>14</sup>B. Chehroudi, D. Talley, and E. Coy, "Visual characteristics and initial growth rates of round cryogenic jets at subcritical and supercritical pressures," *Phys. Fluids* **14**, 850 (2002).
- <sup>15</sup>R. S. Miller, "Long time mass fraction statistics in stationary compressible isotropic turbulence at supercritical pressure," *Phys. Fluids* **12**, 2020 (2000).
- <sup>16</sup>H. Lou and R. S. Miller, "On the scalar probability density function transport equation for binary mixing in isotropic turbulence at supercritical pressure," *Phys. Fluids* **13**, 3386 (2001).
- <sup>17</sup>K. Denbigh, *The Principles of Chemical Equilibrium* (Cambridge University Press, Cambridge, England, 1981).
- <sup>18</sup>H. Lou, Ph.D. dissertation, Clemson University, Department of Mechanical Engineering, 2002.
- <sup>19</sup>S. Sarman and D. J. Evans, "Heat flow and mass diffusion in binary Lennard-Jones mixtures," *Phys. Rev. A* **45**, 2370 (1992).
- <sup>20</sup>S. Kida and S. A. Orszag, "Energy and spectral dynamics in forced compressible turbulence," *J. Sci. Comput.* **5**, 85 (1990).
- <sup>21</sup>C. A. Kennedy and M. H. Carpenter, "Several new numerical methods for compressible shear-layer simulations," *Appl. Numer. Math.* **14**, 397 (1994).
- <sup>22</sup>R. S. Miller and J. Bellan, "On the validity of the assumed PDF method for modeling binary mixing/reaction of evaporated vapor in gas/liquid-droplet turbulent shear flow," *Proceedings of the 27th Symposium (International) on Combustion* (1998), pp. 1065-1072.
- <sup>23</sup>R. S. Miller and J. Bellan, "Direct numerical simulation of a confined three-dimensional gas mixing layer with one evaporating hydrocarbon-droplet laden stream," *J. Fluid Mech.* **384**, 293 (1999).
- <sup>24</sup>R. S. Miller and J. Bellan, "Direct numerical simulation and subgrid analysis of a transitional droplet laden mixing layer," *Phys. Fluids* **12**, 650 (2000).